

# A soft X-ray study of type I active galactic nuclei observed with *Chandra* high-energy transmission grating spectrometer

B. McKernan,<sup>1,2★</sup> T. Yaqoob<sup>3,4</sup> and C. S. Reynolds<sup>5</sup>

<sup>1</sup>*Department of Science, Borough of Manhattan Community College, City University of New York, New York, NY 10007, USA*

<sup>2</sup>*Hayden Associate, Hayden Planetarium, Department of Astrophysics, American Museum of Natural History, New York, NY 10024, USA*

<sup>3</sup>*Department of Physics and Astronomy, Johns Hopkins University, Baltimore, MD 21218, USA*

<sup>4</sup>*Laboratory for High Energy Astrophysics, NASA/Goddard Space Flight Center, Greenbelt, MD 20771, USA*

<sup>5</sup>*Department of Astronomy, University of Maryland, College Park, MD 20742, USA*

Accepted 2007 May 14. Received 2007 May 11; in original form 2006 August 30

## ABSTRACT

We present the results of a uniform analysis of the soft X-ray spectra of 15 type I active galactic nuclei (AGN) observed with the high-resolution X-ray gratings onboard *Chandra*. We found that 10 out of the 15 AGN exhibit signatures of an intrinsic ionized absorber. The absorbers are photoionized and outflowing, with velocities in the range  $\sim 10^1 - 10^3$  km s<sup>-1</sup>. The column density of the warm absorbing gas is  $\sim 10^{20-23}$  cm<sup>-2</sup>. Nine out of the 10 AGN exhibiting warm absorption are best fitted by multiple ionization components and three out of the 10 AGN *require* multiple kinematic components. The warm absorbing gas in our AGN sample has a wide range of ionization parameter, spanning roughly four orders of magnitude ( $\xi \sim 10^{0-4}$  erg cm s<sup>-1</sup>) in total, and often spanning three orders of magnitude in the same gas. Warm absorber components with ionization parameter  $\xi < 10$  generate an unresolved transition array due to Fe in seven out of the 10 AGN exhibiting warm absorption. These low ionization state absorbers may also carry away the largest mass outflows from the AGN. The mass outflow rate depends critically on the volume filling factor of the gas, which cannot yet be directly measured. However, upper limits on the mass outflow rates for filling factors of unity can be much greater than the expected accretion rate on to the central supermassive black hole and filling factors as small as 1 per cent can give outflow rates comparable to the accretion rate. There appears to be a gap in the outflow velocities in our sample between  $\sim 300$  and  $500$  km s<sup>-1</sup>, the origin of which is not clear. The outflow components with velocities below this gap tend to be associated with lower column densities than those with velocities above the gap.

**Key words:** techniques: spectroscopic – Galaxy: disc – galaxies: active – galaxies: Seyfert – X-rays: galaxies.

## 1 INTRODUCTION

X-ray emission from active galactic nuclei (AGN) is believed to be powered by an accretion flow on to a supermassive black hole (SBH). In the unified AGN paradigm, type I AGN have accretion discs at a small angle of inclination to the observers' line of sight. Hard X-ray ( $>2$  keV) spectra from type I AGN typically reveal a continuum that is well described by a simple cut-off power-law model, with a fluorescent Fe K line complex (and sometimes a reflection continuum) superimposed (see e.g. Reynolds & Nowak 2003 and references therein). The soft X-ray ( $<2$  keV) spectra of type I AGN are typically complex and can yield a great deal of

information about the distribution and state of matter in the AGN central engine.

Spectral complexity beyond a simple power-law model in the soft X-ray spectrum of an AGN was first observed in MR 2251–178 Halpern (1984). The spectral complexity was due to absorption by partially ionized, optically thin, circumnuclear material. This material, termed the 'warm absorber' was proposed as a common constituent of many AGN. *ROSAT* observations of nearby type I AGN showed that warm absorption was not uncommon, see, for example, (Nandra & Pounds 1992; Turner et al. 1993). Subsequent observations with *ASCA* detected O VII and O VIII absorption edges due to warm absorption in  $\sim 50$  per cent of type I AGN (Reynolds 1997; George et al. 1998). Observations in the ultraviolet (UV) band reveal warm absorption with multiple velocity components and ionization states, although the relationship between the UV absorbers and the

★E-mail: mckernan@astro.umd.edu

**Table 1.** The *Chandra* HETGS sample of type I AGN. AGN are listed in order of increasing RA. Columns 2–4 give the coordinates and the redshift of the source (from NED). Redshift was deduced from observations of the 21-cm H I line where possible, since optical estimates of  $z$  may be confused by AGN outflow. Column 7 is the mean count rate for the combined  $\pm 1$  order spectra of the MEG.

Source	RA (J2000.0)	Dec. (J2000.0)	Redshift ( $z$ )	Galactic $N_{\text{H}}$ ( $10^{20} \text{ cm}^{-2}$ ) <sup>a</sup>	Observation start <sup>b</sup>	MEG count rate (counts s <sup>-1</sup> )	Exposure <sup>c</sup> (ks)
Fairall 9	01 23 45.7	−58 48 21	0.046 00	3.0	2001 September 11	0.486 ± 0.02	80
3C 120 <sup>d</sup>	04 33 11.0	05 21 15	0.033 01	12.30	2001 December 21	0.814 ± 0.004	58
NGC 3227	10 23 30.6	+19 51 54	0.003 86	2.15	1999 December 30	0.130 ± 0.003	47
NGC 3516	11 06 47.5	+72 34 07	0.008 84	3.05	2001 April 9		36
					2001 April 10	0.132 ± 0.002 <sup>f</sup>	75
					2001 November 11	0.230 ± 0.003	89
NGC 3783	11 39 01.7	−37 44 18	0.009 73	8.50	2001 February 24	0.668 ± 0.002	850
NGC 4051	12 03 09.5	44 31 52	0.002 42	1.31	2000 March 24	0.396 ± 0.002	80
Mkn 766	12 18 26.5	29 48 46	0.012 93	1.80	2001 May 7	0.572 ± 0.002	90
NGC 4593 <sup>e</sup>	12 39 39.3	−05 20 39	0.008 31	1.97	2001 June 29	0.948 ± 0.004	79
MCG-6-30-15 <sup>e</sup>	13 35 53.3	−34 17 48	0.007 75	4.06	2000 April 5	0.594 ± 0.002	126
IC 4329A <sup>e</sup>	13 49 19.2	−30 18 34	0.016 05	4.55	2001 August 26	2.244 ± 0.006	60
Mkn 279	13 53 03.5	+69 18 30	0.030 45	1.64	2002 May 18	0.241 ± 0.002	116
NGC 5548 <sup>e</sup>	14 17 59.5	25 08 12	0.017 17	1.70	2000 February 5	0.403 ± 0.002	82
Mkn 509 <sup>e</sup>	20 44 09.6	−10 43 23	0.034 40	4.44	2001 April 13	0.963 ± 0.004	60
NGC 7314	22 35 46.2	−26 03 01	0.004 74	1.46	2002 July 19	0.353 ± 0.002	97
Akn 564	22 42 39.3	29 43 31	0.024 67	6.40	2000 June 17	1.302 ± 0.007	50

<sup>a</sup>From Elvis et al. (1989), except for Mkn 509 Murphy et al. (1996). The Galactic column density towards F9, NGC 7314, 3516, 3783, 5548, Mkn 766, NGC 3227 and Akn 564 was obtained from Reynolds (1997). <sup>b</sup>NGC 3516: Dates of three ‘snapshots’ are given; NGC 3783: data were combined from five observations over a period of  $\sim 124$  d; MCG-6-30-15: this observation was made over a period of  $\sim 138$  d in three parts and only the combined data are analysed here. <sup>c</sup>Total good integration time of spectrum. <sup>d</sup>3C 120 is also classified as a broad-line radio galaxy (NED). <sup>e</sup>To gauge changes in AGN spectral continua, particularly in the vicinity of the oxygen absorption edges, the *XMM-Newton* EPIC PN spectrum of this AGN was studied. <sup>f</sup>We summed the first two observations of NGC 3516 into a single ‘low-state’ spectrum and compared this with the ‘high-state’ spectrum in the third observation.

X-ray absorbers is still not clear (Crenshaw & Kraemer 1999; Arav, Korista & de Kool 2002). The unprecedented spectral resolution of the gratings onboard *Chandra* and *XMM-Newton* has permitted the detection of discrete soft X-ray absorption features and emission lines for the first time. The resulting picture of the X-ray warm absorber in many type I AGN is of an outflow exhibiting multiple narrow absorption lines corresponding to different ionization states, for example, (Collinge et al. 2001; Lee et al. 2001; Sako et al. 2001; Kaastra et al. 2002; McKernan et al. 2003a; Netzer et al. 2003; Yaqoob et al. 2003). The present generation of X-ray detectors also have the spectral resolution to detect unresolved transition arrays (UTAs) in moderately ionized iron ( $\text{Fe}^{0-15}$ ) in several AGN spectra (Sako et al. 2001; Behar, Sako & Kahn 2001; Blustin et al. 2002; Pounds et al. 2003).

Our picture of the X-ray warm absorber is now more complicated, and many fundamental questions remain. Does the warm absorber ‘know’ about the SBH mass, for example, Morales & Fabian (2002), the accretion rate, or the AGN luminosity? Does radiation pressure dominate the warm absorber outflow? Is there a link between the warm absorber and the Fe K band emission, for example, Matt (1994)? Only via the analysis of the soft X-ray spectra of a sample of type I AGN can we answer such questions. Here we present the results of a uniform analysis of the soft X-ray data from a sample of 15 type I AGN observed with the high-energy transmission grating spectrometer (HETGS) onboard *Chandra* (Markert et al. 1995). Our aim is to study the soft X-ray spectra of these AGN so that we may begin to answer some of the outstanding questions about warm absorption in AGN. Of course our study is limited by both our choice of sample and X-ray instrument. The *Chandra* HETGS bandpass is less sensitive to low ionization state absorbers than the *Chandra* LETGS bandpass for example. Both the LETGS and the

RGS (aboard *XMM-Newton*) have a higher effective area than the MEG at low energies but the HETGS spectral resolution is superior to both the LETGS and RGS. Utilizing the best spectral resolution currently available is the principal driving factor for using the HETGS in the present study. There are many more HETGS observations than LETGS observations and the RGS bandpass does not extend to the Fe K region of AGN spectra. We note that in a uniform analysis, individual source peculiarities (e.g. in the continuum modelling) may be missed. An additional complication is that the absorbers in some AGN are known to vary, so drawing general conclusions based on a snapshot of a variable absorber may not be warranted in some cases. Nevertheless, a uniform analysis is useful since variations between analysis software and/or methodologies can account for considerable differences in interpretation, often over the same data.

## 2 THE SAMPLE AND DATA ANALYSIS

Our study is based on the sample of 15 type I AGN selected by Yaqoob & Padmanabhan (2004). The AGN listed in Table 1 were originally assembled for a study of the Fe K band emission and had  $z < 0.05$ , a total, first-order, high-energy grating (HEG) count rate of  $> 0.05$  counts s<sup>-1</sup> and the observations were in the *Chandra* public data archive<sup>1</sup> as of 2003 July 1. This constitutes a rather heterogeneous sample that is not based on a scientifically motivated selection criterion. Therefore, certain results and conclusions pertaining to *sample* properties (such as the fraction of AGN exhibiting signatures of photoionized outflows) must be interpreted with the

<sup>1</sup> <http://cda.harvard.edu/chaser/mainEntry.do>.

appropriate caution. However, members of the sample do satisfy one very important criterion relevant for this study, namely, that these sources are some of the brightest members of their class and therefore lend themselves to performing detailed X-ray spectroscopy with the *Chandra* HETGS. This is not a coincidence because generally speaking, the highest signal-to-noise ratio (S/N) members of a class tend to get accepted first by selection panels for observations in the early years of a new mission.

We note that several of the AGN listed in Table 1 have been observed with *Chandra* again (for which that data became public after 2003 July 1). Furthermore, an additional 13 AGN have been observed with the *Chandra* gratings that would fulfil the selection criteria of Yaqoob & Padmanabhan (2004). In the future we intend to extend our sample study to include these AGN and more recent observations of the AGN in our sample. Also listed in Table 1 are the AGN redshifts [from NASA/IPAC Extragalactic Database (NED)<sup>2</sup> using 21 cm HI radiation measurements where possible], the right ascension (RA) and declination (Dec.) (also from NED), the Galactic column density (Elvis, Wilkes & Lockman 1989; Murphy et al. 1996) and the total exposure times of the spectra.

The *Chandra* data were reprocessed using CIAO 2.1.3 and CALDB version 2.7, according to recipes described in CIAO 2.1.3 threads.<sup>3</sup> The instrument in the focal plane of *Chandra* during the observations was the HETGS, which consists of two grating assemblies, an HEG and a medium energy grating (MEG). Only the summed, negative and positive, first-order *Chandra* grating spectra were used in our analysis. The HEG bandpass is  $\sim 0.8$ – $10$  keV and the MEG bandpass is  $\sim 0.5$ – $10$  keV but the effective area of both instruments falls off rapidly at either end of the bandpass. Since the MEG soft X-ray response is much better than the HEG we used the MEG as the primary instrument.

We made effective area files (ARFs or *ancillary response files*), photon spectra and counts spectra following the method of Yaqoob et al. (2003). We did not subtract detector or X-ray background since it is such a small fraction of the observed counts. For spectra with zero or few counts per bin anywhere in the bandpass, attempting to subtract background whilst retaining the best spectral resolution possible can result in worse systematic errors compared to the case when no background subtraction is attempted. This is especially true when the background itself is weak, having zero counts for most spectral bins. However, background could be a source of contamination at the lowest energies of the MEG spectra (where the effective area is the smallest), for weak and/or heavily absorbed sources. We examined spectra taken from two strips, either side of the on-source data, to check the level of background for each data set. We found that contamination could be a problem in NGC 3516, 3227 and 7314, where the background level becomes comparable to the source intensity below  $\sim 0.6$  keV. We will bear this in mind when interpreting the data. We note that five out of the 15 AGN in our sample were observed with the *Chandra* low-energy transmission grating spectrometer (LETGS). The high-resolution camera (HRC) was used in four of these five LETGS observations (as opposed to ACIS). However, order separation is not possible with the HRC and the properties of the LETGS are considerably different to those of the HETGS [e.g. LETGS has a lower spectral resolution of only  $0.05$  Å full width at half-maximum (FWHM) and so inclusion of the LETGS data would have complicated efforts to perform a uniform analysis and comparison amongst the sources. Note

that the observations of three of the AGN (NGC 3516, 3783 and MCG-6-30-15) were not made in a single observing period. NGC 3516 was observed in three parts, as detailed in Table 1. However, two of the observations found NGC 3516 in a low-flux state. So, in our analysis of the warm absorber in this AGN, we summed two of the observations into a single ‘low-state’ spectrum and compared this with the ‘high-state’ spectrum in the third observation. NGC 3783 was observed in five snapshots over a period of  $\sim 124$  d. However, we analyse only the summed data in the present paper, since the spectral variability, which has been studied in detail by Netzer et al. (2003) is not great. The observation of MCG-6-30-15 has a single sequence number and observation ID, but was made in three parts, spanning a period of  $\sim 138$  d. The S/N in the individual parts was not sufficient to warrant analysing the three parts separately so here we analyse only the summed data.

For comparison with some of the results from the *Chandra* observations, we studied *XMM-Newton* spectra from some of the AGN in our sample. We used observations made with the *XMM-Newton* EPIC PN instrument. The data used were obtained from the reduced data products from the Xassist data base.<sup>4</sup> AGN in our HETGS sample with corresponding *XMM-Newton* observations are listed in Table 1.

We treated the statistical errors on both the photon and counts spectra with particular care since the lowest and highest energies of interest can be in the Poisson regime, with spectral bins often containing a few, or even zero counts. When plotting data, we assign statistical upper and lower errors of  $1.0 + \sqrt{(N + 0.75)}$  and  $N/[1.0 - \{1.0 - [1/(9N)] - 1/(3\sqrt{N})\}^3]$ , respectively (Gehrels 1986) on the number of photons,  $N$ , in a given spectral bin. When fitting the *Chandra* data, we used the  $C$  statistic (Cash 1976) for finding the best-fitting model parameters, and quote 90 per cent confidence, one-parameter statistical errors unless otherwise stated. The  $C$  statistic minimization algorithm is inherently Poissonian and so makes no use of the errors on the counts in the spectral bins described above. All model parameters will be referred to the source frame, unless otherwise noted. Note that since all models were fitted by first folding through the instrument response before comparing to the data, the derived model parameters *do not* need to be corrected for instrumental response.

We used XSPEC v.11.3.1 for spectral fitting to the HETGS spectra. All spectral fitting was done in the  $0.5$ – $5$  keV energy band, excluding the  $2.0$ – $2.5$  keV region, which suffers from systematics as large as  $\sim 20$  per cent in the effective area due to limitations in the calibration of the X-ray telescope.<sup>5</sup> We performed spectral fits using data binned at  $\sim 0.02$  Å (which is close to the MEG FWHM spectral resolution of  $0.023$  Å), unless otherwise stated. There has been a continuous degradation of the quantum efficiency of *Chandra* ACIS with time, due to molecular contamination.<sup>6</sup> In analyses of individual sources (McKernan et al. 2003a,b; Yaqoob et al. 2003) we found that a pure ACIS correction (the worst case effect) affects only the inferred intrinsic continuum (at less than  $\sim 0.7$  keV) and does not affect the important physical parameters of warm absorber models. A detailed comparison of spectral results with and without the ACIS degradation correction was given in (McKernan et al. 2003a) for the case of NGC 4593. We also note that the data in our sample are from early in the *Chandra* mission when the ACIS degradation was

<sup>2</sup> <http://nedwww.ipac.caltech.edu>.

<sup>3</sup> <http://cxc.harvard.edu/ciao/threads>.

<sup>4</sup> <http://xassist.pha.jhu.edu>.

<sup>5</sup> [http://cxc.harvard.edu/cal/cal\\_present\\_status.html](http://cxc.harvard.edu/cal/cal_present_status.html).

<sup>6</sup> [http://cxc.harvard.edu/cal/Acis/Cal\\_prods/qeDeg/index.html](http://cxc.harvard.edu/cal/Acis/Cal_prods/qeDeg/index.html).

**Table 2.** Best-fitting simple broken power-law continuum parameters (including neutral absorption with column density  $N_{\text{H}}$ , covering a fraction, CF, of the source), and observed 0.5–2 keV fluxes. The broken power law has photon indices  $\Gamma_1$  and  $\Gamma_2$ , and a break energy  $E_{\text{B}}$ .

Source	Cold $N_{\text{H}}$ ( $10^{20} \text{ cm}^{-2}$ )	CF	$\Gamma_1$	$E_{\text{B}}$ (keV)	$\Gamma_2$	Flux (0.5–2.0 keV) ( $10^{-12} \text{ erg cm}^{-2} \text{ s}^{-1}$ )
F9	<1		$2.10^{+0.09}_{-0.07}$	$1.06^{+0.08}_{-0.04}$	$1.78^{+0.02}_{-0.03}$	11.9
3C 120	<1		$1.79^{+0.11}_{-0.10}$	$0.99^{+0.29}_{-0.16}$	$1.68 \pm 0.03$	16.8
NGC 3227	$188 \pm 24$	$0.84^{+0.04}_{-0.05}$			$1.32^{+0.19}_{-0.18}$	1.6
NGC 3516 (low)	$247^{+15}_{-17}$	$0.82^{+0.04}_{-0.03}$			$1.65^{+0.10}_{-0.12}$	2.0
NGC 3516 (high)	$213^{+21}_{-19}$	$0.79^{+0.02}_{-0.03}$			$1.92^{+0.11}_{-0.13}$	3.7
NGC 3783	$102^{+1}_{-2}$	$0.75 \pm 0.01$	$3.07^{+0.05}_{-0.06}$	$1.23 \pm 0.01$	$1.92^{+0.02}_{-0.03}$	11.8
NGC 4051	<1		$3.08^{+0.14}_{-0.07}$	$1.23^{+0.03}_{-0.09}$	$1.77 \pm 0.05$	12.6
Mkn 766	$2 \pm 1$		$3.10^{+0.16}_{-0.28}$	$0.91^{+0.08}_{-0.04}$	$1.85^{+0.03}_{-0.04}$	15.0
NGC 4593	$3^{+2}_{-1}$		$2.72^{+0.19}_{-0.16}$	$0.96^{+0.05}_{-0.02}$	$1.80 \pm 0.04$	20.9
MCG-6-30-15	$6 \pm 2$		$3.82^{+0.24}_{-0.21}$	$1.02^{+0.04}_{-0.02}$	$1.76^{+0.04}_{-0.05}$	9.7
IC 4329A	$32^{+4}_{-3}$		$3.66^{+0.28}_{-0.22}$	$0.98 \pm 0.03$	$1.83^{+0.02}_{-0.03}$	77.9
Mkn 279	<1		$1.96^{+0.17}_{-0.16}$	$0.89^{+0.14}_{-0.09}$	$1.56 \pm 0.03$	5.6
NGC 5548	<1		$2.80^{+0.16}_{-0.13}$	$0.95 \pm 0.03$	$1.46^{+0.04}_{-0.03}$	10.0
Mkn 509	<1		$2.50^{+0.08}_{-0.09}$	$0.96^{+0.09}_{-0.06}$	$1.63 \pm 0.03$	23.1
NGC 7314	$107 \pm 5$	$0.97 \pm 0.01$			$2.00^{+0.06}_{-0.05}$	4.9
Akn 564	$4^{+2}_{-1}$		$3.16^{+0.11}_{-0.15}$	$1.43^{+0.06}_{-0.05}$	$2.48 \pm 0.05$	44.9

not so severe and the effects of the degradation are mitigated by the limited S/N of the data at the lowest energies.

### 3 THE OVERALL SOFT X-RAY SPECTRA

The soft X-ray continua of type I AGN can be quite complex. An excess over a simple power-law continuum model, as well as possible absorption features, are common. In our sample, nine out of the 15 AGN in Table 1 show features characteristic of a soft excess and/or absorption edges. NGC 3227, 3516, IC 4329A and NGC 7314 are heavily absorbed in the soft X-ray band. F9, 3C 120 and Mkn 279 have relatively simple continua, since their spectra show little or no evidence for a soft excess. Since the soft excess typically appears only in the 0.5–0.7 keV band of our data, we do not have enough information to constrain its origin and so sophisticated modelling of the continuum (such as with a power-law plus a blackbody model component) is not warranted. We found that a broken power law (although likely to be non-physical) is adequate to describe the intrinsic continuum including any soft excess in the HETGS energy band. When partially covering cold absorption is added to the model a useful empirical description of the overall spectra is obtained, leaving residuals mostly due to complex, ionized absorption, and in some cases some emission lines. Table 2 shows the best-fitting parameters obtained with this model for each source, as well as observed 0.5–2 keV fluxes.

### 4 PHOTOIONIZATION MODELLING OF THE AGN WARM ABSORBERS

We used the publicly available photoionization code *xstar* 2.1.kn3<sup>7</sup> to generate several grids of models of emission and absorption from photoionized gas in order to directly compare with the data. Version 2.1.kn3 includes UTAs of inner-shell transitions of Fe for the first

time in *xstar*. It is important to include UTAs in our photoionized model grids since they provide the key to studying low ionization state absorbers in AGN and UTAs of moderately ionized  $\text{Fe}^{0-15+}$  have been observed in the spectra of several type I AGN (see e.g. Behar et al. 2001; Sako et al. 2001; Blustin et al. 2002; Pounds et al. 2003). We used the default solar abundances in *xstar* (e.g. see table 2 in Yaqoob et al. 2003). Note that the *xstar* line data base has been constructed from lines with published wavelengths, such as the Chianti line compilation.<sup>8</sup> This almost completely excludes the lines listed in Behar & Neztzer (2002) for example, which are based on HULLAC calculations and which are only reliable at about the 1 per cent level. These lines, due to L-shell transitions in Ne, Mg, Al, Si, S, Ar, Ca and Fe, are present in many *Chandra* grating spectra (see e.g. Neztzer et al. 2003), but so far they have mostly been omitted from the *xstar* data base rather than compromise the accuracy of the data base (Kallman, private communication).

There may be additional absorption in most of these AGN, beyond the simple photoionized warm absorber models that we consider in this uniform analysis. Candidates for the extra absorption include neutral dust (e.g. possibly in the form of  $\text{FeO}_2$  in MCG-6-30-15, see Lee et al. 2001) or deeper O VII or O VIII edges due to oxygen overabundance. Alternatively, a more complex model of the continuum may be more appropriate, incorporating relativistically broadened emission lines in the soft X-ray band (see e.g. Branduardi-Raymont et al. 2001; Mason et al. 2003; Sako et al. 2003). However, investigation of these issues is beyond the scope of the present uniform analysis and we shall return to these important points in future work.

The best spectral resolution of the MEG cannot *directly* constrain turbulent velocities with a ‘*b*-value’ of less than  $170 \text{ km s}^{-1}$ . Furthermore, the *xstar* model spectra are calculated by *xstar* on a grid that does not always preserve accuracy in the linewidths and line equivalent widths (EWs) (Kallman, private communication).

<sup>7</sup> <http://heasarc.gsfc.nasa.gov/docs/software/xstar/xstar.html>.

<sup>8</sup> <http://www.solar.nrl.navy.mil/chianti.html>.

Therefore, direct fits to the data using the XSTAR spectra are approximate in the regions containing absorption lines. However, the ionic column densities output by the XSTAR are more accurate than the XSTAR spectra and can be used for more detailed modelling of individual absorption lines. This level of detail is beyond the scope of the present uniform analysis. We used a velocity turbulence ( $b$ -value) of  $170 \text{ km s}^{-1}$ , which corresponds approximately to the limiting MEG spectral resolution ( $\sim 300 \text{ km s}^{-1}$  FWHM at  $0.5 \text{ keV}$ ), given that the data cannot directly constrain smaller linewidths. It is possible to constrain  $b$  using a curve-of-growth analysis if one has several absorption-line measurements, and this has been done for some of the sources in our sample in more detailed studies. For example, in Mkn 509  $b$  is consistent with  $\sim 100 \text{ km s}^{-1}$  (Yaqoob et al. 2003), with similar results obtained for other sources. Since  $b$  is generally comparable to or less than the spectral resolution, our adopted value of  $b$  is justified for the purpose of spectral fitting.

#### 4.1 XSTAR modelling procedure

First, we constructed a spectral energy distribution (SED) for each AGN in our sample, according to the method described in Yaqoob et al. (2003). In principle, derivation of the SED should be an iterative process since the intrinsic X-ray spectrum is obtained from fitting the data using an SED that must already contain information about the X-ray spectrum. In practice, the method employed (described in Yaqoob et al. (2003)) is a two-step process in which the first step is an initial estimate of the intrinsic X-ray spectrum is obtained by fitting the X-ray data with a power law or broken power law only and no photoionized absorber. The resulting estimated SED is used to generate grids of photoionization models that are used to obtain better fits to the data and to derive a new intrinsic X-ray spectrum. This is then used to generate another SED which is in turn used to generate a new set of photoionization model grids and the latter are the ones used for the final model fits. Average radio, infrared (IR), optical and UV fluxes were obtained from Ward et al. (1987) and NED. Note that flux measurements, at different wavelengths, obtained from historical data (Ward et al. 1987, NED) are not in general contemporaneous. For each source, the  $0.5 \text{ keV}$  intrinsic model flux from the intrinsic X-ray continuum model was then simply joined on to the last point of the UV part of the SED by a straight line in log-log space. The hard X-ray power law was extended out to  $100 \text{ keV}$ . Generally, the high-energy cut-off in the observed X-ray spectra of Seyfert galaxies lies in the range  $100\text{--}500 \text{ keV}$ ; only blazars and BL Lacs are observed to have significant flux beyond  $500 \text{ keV}$ . The ionization balance is not sensitive to the exact position of the cut-off between  $100\text{--}500 \text{ keV}$ . At the low-energy end, it has been shown (e.g. by Ferland et al. 2002) that if the observed IR continuum carries a significant thermal component from reprocessing of the intrinsic continuum, using the observed SED as an input to photoionization models can potentially affect the resulting ionization balance of the plasma. However, our model fits are driven by X-ray features and we showed in a detailed study of NGC 4593 (McKernan et al. 2003a) that removing the prominent IR-optical continuum bump from the SED yielded warm absorber parameters that were within the 90 per cent confidence intervals obtained when the bump was not removed. Fig. 1 shows the SEDs that we used for the 10 AGN in our sample that exhibited warm absorption (see Section 4.2 below).

The photoionization model grids used here are two dimensional, corresponding to a range in values of total neutral hydrogen column density,  $N_{\text{H}}$ , and the ionization parameter,  $\xi = L_{\text{ion}}/(n_e R^2)$ . Here  $L_{\text{ion}}$  is the ionizing luminosity in the range  $1\text{--}1000 \text{ Ryd}$ ,  $n_e$  is the

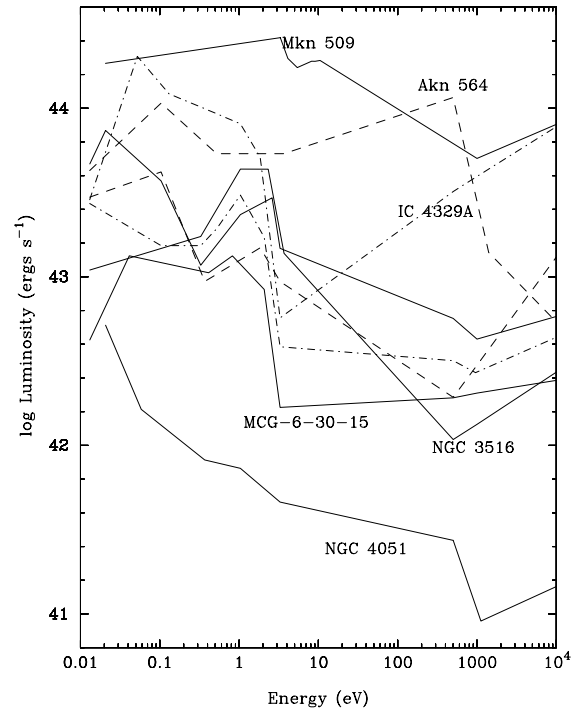


**Figure 1.** SEDs used for photoionization modelling to the *Chandra* data of 10 AGN in our sample (see Section 4.1). In order of decreasing luminosity at  $10 \text{ keV}$  (right-hand side of graph), the SEDs correspond to Mkn 509, IC 4329A, NGC 5548, 3783, Mkn 766, Akn 564, NGC 4593, 3516, MCG-6-30-15 and NGC 4051, respectively.

electron density and  $R$  is the distance of the illuminated gas from the ionizing source. The ionizing luminosities were calculated from the SEDs by normalizing the absorption-corrected  $0.5\text{--}2 \text{ keV}$  fluxes. The grids were computed for equispaced intervals in the logarithms of  $N_{\text{H}}$  and  $\log \xi$ , in the ranges  $10^{19}\text{--}5 \times 10^{23} \text{ cm}^{-2}$  and  $-1.0$  to  $+4.0 \text{ erg cm s}^{-1}$ , respectively. We computed grids with  $n_e$  in the range  $10^2\text{--}10^{11} \text{ cm}^{-3}$ . For XSTAR models of the *absorber*, we confirmed that results from fitting the photoionization models to the X-ray data were indistinguishable for densities in the range  $n_e = 10^2$  to  $10^{11} \text{ cm}^{-3}$  for all of the AGN. Hereafter we will use  $n_e = 10^8 \text{ cm}^{-3}$  unless otherwise stated.

Our aim was to fit the MEG spectra with a simple power-law or a broken power-law continuum (whichever was the better fit), modified by absorption from photoionized gas (derived from the AGN SED), neutral gas intrinsic to the AGN and Galactic absorption. All model fittings to the data were carried out using XSPEC v11.3.1. In order to fit XSTAR photoionization model grids to the data, we required an offset velocity for the warm absorber for each of the AGN. Therefore, first we tested for the following He- and H-like absorption lines in each spectrum within  $\sim \pm 5000 \text{ km s}^{-1}$  of the line rest energy in the AGN frame: N VII Ly $\alpha$  ( $\lambda 24.781 \text{ \AA}$ ), O VII (r) ( $\lambda 21.602 \text{ \AA}$ ), O VIII Ly $\alpha$  ( $\lambda 18.969 \text{ \AA}$ ), Ne IX (r) ( $\lambda 13.447 \text{ \AA}$ ), Ne X Ly $\alpha$  ( $\lambda 12.134 \text{ \AA}$ ), Mg XI (r) ( $\lambda 9.169 \text{ \AA}$ ), Mg XII Ly $\alpha$  ( $\lambda 8.421 \text{ \AA}$ ), Si XIII (r) ( $\lambda 6.648 \text{ \AA}$ ), Si XIV Ly $\alpha$  ( $\lambda 6.182 \text{ \AA}$ ). Note that for individual absorption features, the statistical errors on the line energies are typically very small and so the systematic uncertainty likely dominates these errors. The relative wavelength accuracy of the MEG is  $0.0055 \text{ \AA}$  and the absolute wavelength accuracy of the MEG is  $0.011 \text{ \AA}$ .<sup>9</sup>

<sup>9</sup> <http://asc.harvard.edu/proposer/POG/html/HETG.html>.

Next, we established an offset velocity for a particular AGN by finding the weighted mean offset velocity (and the 90 per cent confidence limits) of the centroids of all the absorption lines detected at >90 per cent significance in the spectrum. Some AGN exhibited groups of two or more absorption features separated from another such group by more than the 90 per cent errors on their respective centroid velocities. In these cases, we established more than one weighted mean offset velocity. Finally, we fitted XSTAR models only to those AGN where two or more prominent absorption signatures had similar offset velocities (within 90 per cent confidence limits). This approach has the merit of being uniform, but it runs the risk of being too conservative and we may be biasing our study in favour of more prominent warm absorption signatures. On the other hand, our method *does* have the merit of ignoring statistically spurious features. We tested for the presence of multiple ionization compo-

nents in the absorbers by investigating the statistical significance of additional model components within the 90 per cent confidence limits of the weighted mean offset velocity.

#### 4.2 XSTAR model results

Table 3 lists the best-fitting warm absorber models that we established for our AGN spectra. Figs 2–4 show the best-fitting models overlaid on the HETGS spectra. We note that in Table 3 the derived column densities of each warm absorber component do not depend on the ‘*b*-value’ assumed in the XSTAR models because the absorption lines are unresolved. Also, these column densities are not solely driven by the absorption lines. In particular, in the case of NGC 3783, although our simplistic model gives a poor fit in some regions of the spectrum, missing some absorption lines altogether,

**Table 3.** Detailed spectral fitting results for photoionization models. Column 2 shows the best-fitting cold absorption. Column 5 shows the mean offset velocity (negative = blueshift with respect to systemic) for the warm absorber components. Column 6 shows rate of mass outflow in terms of *C*, the product of the filling factor and the covering factor. Column 7 shows the fit statistic (which includes emission model components from Table 5). Column 8 shows the increase in fit statistic when the absorber component (3 d.o.f.) is removed from the model fit and the model is refitted.<sup>c</sup>The true 90 per cent confidence upper or lower limit could not be determined in these cases. The effective range of the offset velocity should be taken to lie between the best-fitting value and the given upper or lower limit.

Source	$N_{\text{H}}$ ( $10^{20} \text{ cm}^{-2}$ )	$N_{\text{wabs}}$ ( $10^{21} \text{ cm}^{-2}$ )	$\log \xi$ ( $\text{erg cm s}^{-1}$ )	$v_{\text{wabs}}$ ( $\text{km s}^{-1}$ )	$\dot{M}_{\text{out}}/C$ ( $M_{\odot} \text{ yr}^{-1}$ )	<i>C</i> statistic	$\Delta C$
NGC 3516 (low)	$250 \pm 20$	$3 \pm 1$	$2.4^{+0.2}_{-0.1}$	$-910^{+140}_{-155}$	1.1	1363	60
High flux	$210^{+20}_{-30}$	$16^{+8}_{-4}$	$2.5 \pm 0.1$	$-585^{+75}_{-65}$	2.2	1414	131
		$2 \pm 1$	$1.0^{+0.2}_{-0.1}$	$-1685^{+135}_{-170}$	210		18
NGC 3783	$102^{+1}_{-2}$	$20^{+7}_{-3}$	$2.9 \pm 0.1$	$-505 \pm 15$	2.3	9091	689
		$6 \pm 1$	$2.1 \pm 0.1$	$-515 \pm 15$	14		5070
		$2^{+0.2}_{-0.1}$	$0.4 \pm 0.1$	$-545^{+30}_{-20}$	720		1039
		$5^{+0.4}_{-1}$	$3.0 \pm 0.1$	$-1145^{+55}_{-30}$	3.5		696
NGC 4051	<1	$0.1^{+0.1}_{-0.1}$	$1.0 \pm 0.3$	$-520^{+c}_{-90}$	2.5	1296	29
		$0.9^{+0.5}_{-0.3}$	$2.6^{+0.4}_{-0.1}$	$-600^{+90}_{-65}$	0.1		76
		$90^{+40}_{-50}$	$3.8 \pm 0.1$	$-2230^{+50}_{-60}$	< 0.1		41
Mkn 766	$2 \pm 1$	$0.2^{+0.3}_{-0.1}$	< 0.6	$-75^{+25}_{-70}$	310	1289	8
		$0.6^{+1.6}_{-0.5}$	$3.1^{+0.3}_{-0.1}$	$-25^{+c}_{-145}$	< 0.1		6
		$0.2^{+0.3}_{-0.1}$	$2.0 \pm 0.1$	$-25^{+c}_{-25}$	0.4		41
NGC 4593	$3^{+2}_{-1}$	$2 \pm 1$	$2.4^{+0.1}_{-0.2}$	$-95^{+c}_{-10}$	0.3	1393	25
		$4^{+8}_{-2}$	$3.3^{+0.2}_{-0.4}$	$-95^{+c}_{-30}$	< 0.1		43
MCG-6-30-15	$6 \pm 2$	$4 \pm 1$	$0.2 \pm 0.1$	$+30^{+c}_{-60}$	9.1	1673	226
		$3 \pm 1$	$2.1 \pm 0.1$	$+15^{+c}_{-55}$	< 0.1		240
		$30^{+60}_{-20}$	$3.7^{+0.1}_{-0.3}$	$-1555^{+80}_{-130}$	0.2		62
IC 4329a	$32^{+4}_{-3}$	$2.3^{+0.2}_{-0.3}$	$0.2 \pm 0.1$	$-100^{+c}_{-55}$	750	1448	162
		$1.4 \pm 0.3$	$2.2 \pm 0.1$	$-100^{+c}_{-20}$	7.8		175
NGC 5548	<1	$0.6 \pm 0.2$	$2.2 \pm 0.2$	$-560^{+c}_{-80}$	89	1065	126
		$50 \pm 40$	$3.9^{+0.1}_{-0.2}$	$-830^{+270}_{-c}$	3.3		105
Mkn 509	<1	$0.5 \pm 0.2$	$2.3^{+0.2}_{-0.1}$	$-140^{+c}_{-40}$	14	1137	36
		$0.1 \pm 0.1$	$0.6^{+0.8}_{-0.3}$	$-140^{+c}_{-100}$	1100		27
Akn 564	$4^{+1}_{-2}$	$0.1 \pm 0.1$	< 0.4	$-140^{+c}_{-50}$	930	1354	18
		$0.2^{+0.3}_{-0.1}$	$2.6 \pm 0.2$	$-140^{+c}_{-15}$	5.4		131

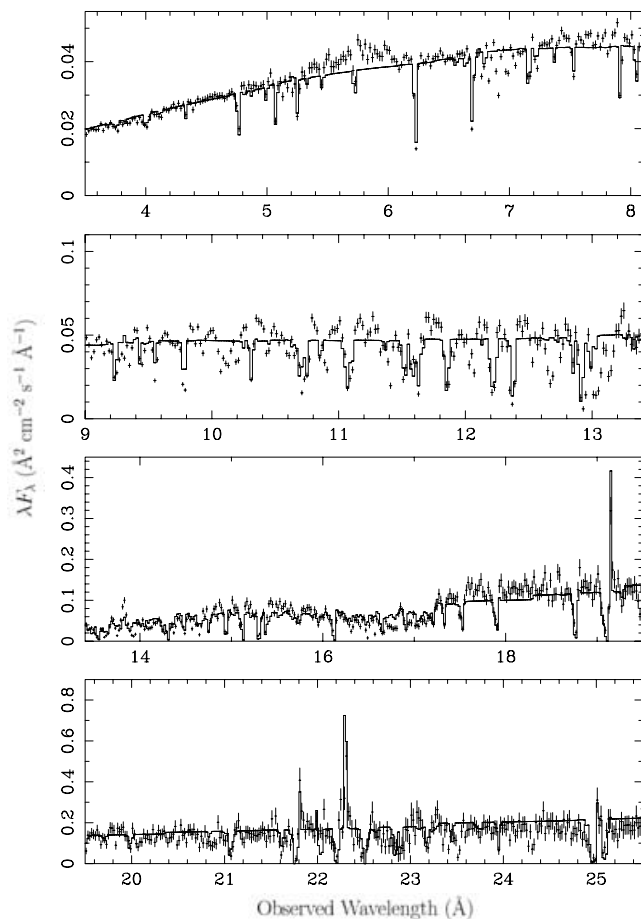


**Figure 2.** MEG-observed photon spectrum compared to the best-fitting simple photoionized absorber plus emitter model (solid line) in the energy range 0.5–3.0 keV for NGC 3783 (see Tables 3 and 5). The data were binned at 0.02 Å for clarity. There are considerable gaps in the *XSTAR* data base of Fe transitions so multiple Fe absorption features are not accounted for by the model. As can be seen, the absence of these lines from the model fit serves to alter the continuum fit in several places. There are also known problems with the fit. The continuum fit is poor around 2.0–2.5 keV ( $\sim 5\text{--}6$  Å) in general due to calibration uncertainties. The continuum excess relative to the model around  $\sim 0.8$  keV ( $\sim 13\text{--}15$  Å) was also found by N03, using a different photoionization code (*ION*) to model the data.

the column densities of the four warm absorber components are not sensitive to this since the four numbers are determined by a fit to tens of absorption lines as well as to the overall spectral shape.

Only 10 out of the 15 AGN in our sample satisfied our criteria for selection and spectral fitting with *XSTAR* grids. AGN F9, 3C 120, Mkn 279, NGC 3227 and 7314 are not included in Table 3. In the case of F9, we found weak O VIII Ly $\alpha$  and O VII (r) absorption signatures ( $\leq 90$  per cent confidence). 3C 120 exhibited strong O VIII Ly $\alpha$  absorption but no other absorption signatures at  $>90$  per cent confidence. In Mkn 279, Ne x Ly $\alpha$  was the only absorption feature present at  $>90$  per cent confidence. In NGC 3227 and 7314, the soft X-ray band was very strongly absorbed, so we could not distinguish between a cold absorber and a mildly warm absorber. In NGC 3227 we only detected a single statistically significant absorption feature (Si xiv Ly $\alpha$  at  $\sim -1700$  km s $^{-1}$  relative to systemic velocity). Note that previous, higher S/N data of the heavily absorbed AGN in our sample (NGC 3227 and 7314) have in some cases detected evidence for photoionized absorption (see e.g. Ptak et al. 1994; Reynolds

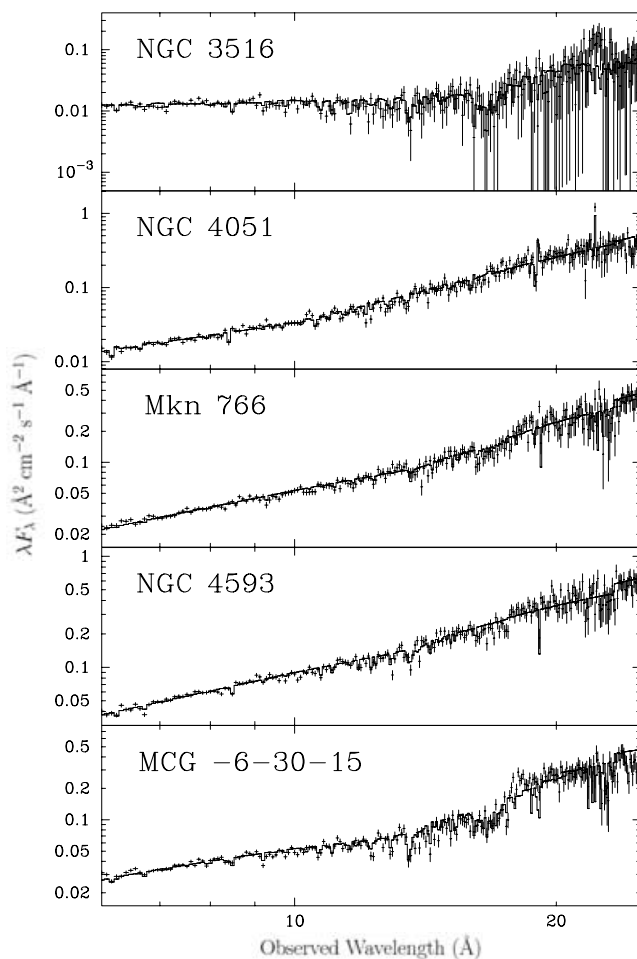


**Figure 3.** MEG-observed photon spectra compared to the best-fitting simple photoionized absorber plus emitter models (solid line) for five of the AGN in our sample (see Tables 3 and 5). The data were binned at 0.08 Å for clarity in the plots (but 0.02 Å for fitting). The plot for NGC 3516 is that for the higher flux state, which is the one that showed evidence for an Fe UTA. Note that the emission feature at  $\sim 0.55$  keV (observed frame) in NGC 3516 is due to the background, not the source (see the text).

1997; George et al. 1998). Spectral plots of the data for the five AGN that are not shown in Fig. 3 can be found in the HETG public data base, HotGAS.<sup>10</sup>

Table 4 shows results from the literature for model fits to X-ray spectra from the AGN in our sample. In general, given the limitations of our methodology, the agreement is actually quite good. Our uniform analysis ignores individual continuum peculiarities in individual AGN and our selection criteria for absorbers are more conservative than many in the literature. In spite of this, our method seems to pick up the same significant absorber components in the literature. Perhaps the best example of this can be seen by comparing our results from NGC 3783 in Table 3 with those from a detailed analysis by Netzer et al. (2003) of the best S/N X-ray spectrum yet. Table 4 shows that Netzer et al. (2003) find two velocity components of the warm absorber with three ionization states. Our simple, uniform method picks out the same velocity components at  $\sim -500$ ,  $-1100$  km s $^{-1}$  and reveals the three ionization states, although we do not establish high velocity components for the middle and low

<sup>10</sup> <http://hotgas.pha.jhu.edu>.

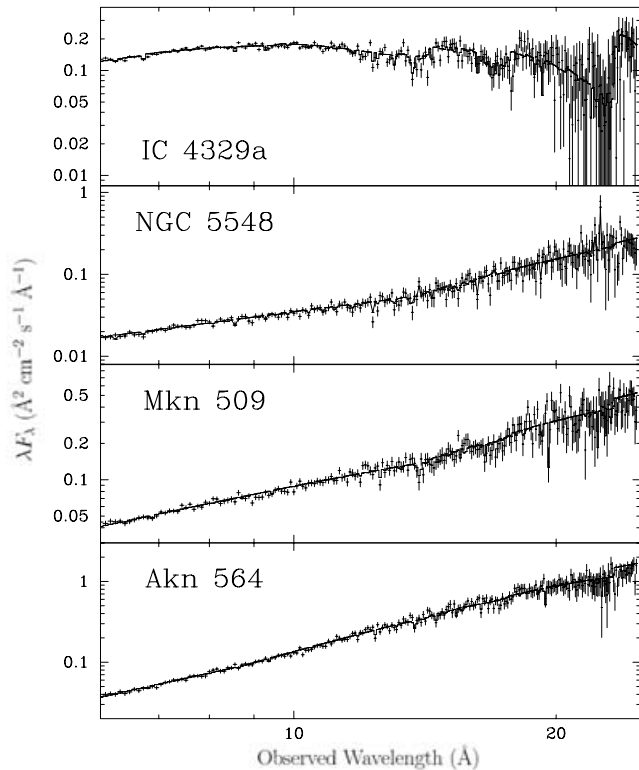


**Figure 4.** As for Fig. 3 for four more of the AGN in our sample.

ionization states. The total column density of the absorbers agrees very well with the value of  $\sim 3 \times 10^{22} \text{ cm}^{-2}$  found by Netzer et al. (2003). Our simple, uniform analysis means that our continuum fit is not as good as that found by Netzer et al. (2003), but it is encouraging that we reproduce most of their model parameters, given that their analysis of this spectrum was far more detailed than ours.

Of course, there are AGN for which individual source peculiarities mean that our results agree less well with those in the literature. In the case of MCG-6-30-15, Lee et al. (2001) and Sako et al. (2003) come to very different conclusions concerning both the origin of the continuum in this AGN *and* the parameters associated with the warm absorber.

UTAs of Fe are a key diagnostic of material in a low-ionization state, which could account for the bulk of the mass outflow from AGN (depending on the absorber density and geometry). The present generation of X-ray telescopes have the spectral resolution to detect blends of Fe inner-shell absorption transitions in the ionized outflows from AGN for the first time. Unresolved arrays of inner-shell (2p–3d) transitions in moderately ionized  $\text{Fe}^{0-15+}$  have been observed in the spectra of several type I AGN (see e.g. Behar et al. 2001, and references therein). Behar et al. (2001) calculate Fe UTAs for an ionization parameter in the range  $\log \xi \sim 0.1 - 1.1$ . The UTA appears as a jagged, broad trough between  $\sim 16$  and  $17 \text{ \AA}$ . As  $\xi$  increases, the centroid of the UTA trough shifts towards shorter wavelengths, the dominant contributions come from more highly ionized states of Fe and the Fe UTA broadens.

Of the 10 AGN in our sample that exhibit signatures of absorption due to photoionized material, only two AGN (NGC 4593 and 5548) did not exhibit statistically significant evidence for a low ionization (Fe UTA) absorber component. Note that in the case of NGC 3516, we only found a low ionization component at statistical significance

in the high-flux state of this AGN. Fig. 5 shows the best-fitting model of the UTA in each of the seven AGN with a warm absorber component where  $\log \xi < 1.1$  (see Table 3). The wavelength scale in Fig. 5 corresponds to the outflowing warm absorber rest frame in each case.

### 4.3 Soft X-ray emission in AGN

As can be seen from Figs 2–4, narrow emission lines were apparent in several of the AGN in our sample. The spectra of NGC 3783, 4051 and 5548 displayed the most prominent narrow lines. Narrow emission lines were less prominent in the spectra of Mkn 279, NGC 4593, Mkn 509 and MCG-6-30-15. The spectra of NGC 3227, 3516 and 7314 showed broad emission features around  $\sim 0.55 - 0.6 \text{ keV}$ . However, the broad emission features in the soft X-ray spectra of these three heavily absorbed AGN were present in the respective background spectra and are therefore not intrinsic to the AGN. We tested for O VII and Ne IX triplet line emission and O VIII Ly $\alpha$  and Ne X Ly $\alpha$  narrow lines in the spectra of the 10 AGN listed above. We followed the fit procedure in Section 4.1 except that the Gaussian model component was not inverted. In a given AGN, we established the weighted mean offset velocity of the centroids of emission lines detected at  $>90$  per cent significance in the spectrum. We then fitted XSTAR emission-line model grids at the mean offset velocity to those AGN spectra displaying multiple ( $>2$ ) emission signatures at  $>99$  per cent significance.

From the definition of  $\xi$ , the emitting material lies at a distance  $R \sim 3 \times 10^{-6} \sqrt{L_{\text{ion},44}/(\xi_{100} n_e)}$  pc from the radiation source, where  $L_{\text{ion},44}$  is the 1–1000 Ryd ionizing radiation from the AGN (in units of  $10^{44} \text{ erg s}^{-1}$ ),  $\xi_{100} = \xi/100 \text{ erg cm}^{-2} \text{ s}^{-1}$  and  $n_e$  is the electron density. For a volume filling factor of unity, the emitting material has a thickness  $\Delta R \sim 1.2 N_{\text{H}}/n_e$  where  $n_e \sim 1.2 n_{\text{H}}$  and  $n_{\text{H}}$  is the density of hydrogen nuclei (assuming  $\text{He}/\text{H} \sim 0.1$  and He contributes two electrons). Therefore, if we assume that  $\Delta R < R$ , then  $n_e > 1.7 N_{21}^2 \xi_{100}/L_{44} \text{ cm}^{-3}$  where  $N_{21} = N_{\text{H}}/10^{21} \text{ cm}^{-2}$ . The best-fitting values of  $N_{\text{H}}$  and  $\xi$  from the XSTAR emission model fits then allow us to establish a lower limit on the electron density in the emitting material. It is important to note however, that the emitting material is not necessarily the same as the absorbing material and therefore may not have the same physical parameters or location as the outflow responsible for absorption.

The three AGN spectra with the most prominent narrow emission lines were NGC 4051, 5548 and 3783. In the spectrum of NGC 4051, the [O VII] and [Ne IX] forbidden lines were the most prominent, with additional emission due to O VIII Ly $\alpha$  and Ne X Ly $\alpha$  and weak O VII (i) emission. There was no apparent O VII (r) emission, indicating that the emitting material in this source is photoionized rather than collisionally ionized. Of course it is also possible that O VII (r) emission may have been re-absorbed by O VII (r) line absorption, which depends on the relative velocity shifts of the emitting and absorbing gases as well as the blending effects of the instrument resolution and the spectral binning. The forbidden lines were marginally blueshifted from systemic velocity and the other (less prominent) emission lines were consistent with emission at systemic velocity. The weighted mean velocity offset of the emission lines in this source ( $-160 \pm 75 \text{ km s}^{-1}$ ) was apparently blueshifted.

NGC 5548 also exhibited strong [O VII] and [Ne IX] forbidden emission lines, with relatively strong O VIII Ly $\alpha$  and O VII (i) emission. O VII (r) line emission was weak in this source, indicating that the emitter is predominantly photoionized rather than collisionally ionized. The He-like Ne and O triplet emission lines in

**Table 4.** Results from the literature for the spectra of the type I AGN in our study. For brevity, we only include the larger studies that parametrized  $N_{\text{H}}$ ,  $\log \xi$  and/or the velocity of the warm absorber. We abbreviated X-ray instruments as: XR = *XMM-Newton* RGS, XE = *XMM-Newton* EPIC-pn, CL = *Chandra* LETGS, CH = *Chandra* HETGS, BX = *BeppoSAX*, RX = *RXTE*. Gaps indicate value of  $\log \xi$  not specified in the literature. In these cases, either no photoionization modelling was carried out (Mkn 766, NGC 4051, 3516) or a different form of the ionization parameter was specified ( $U$  or  $U_{\text{ox}}$ ), with insufficient information to translate to values of  $\log \xi$ .

Source	Instrument	$N_{\text{wabs}}$ ( $10^{21} \text{ cm}^{-2}$ )	$\log \xi$ ( $\text{erg cm s}^{-1}$ )	Velocity $\text{km s}^{-1}$	Reference
NGC 3516	XR	$\sim 8$			Turner et al. (2003)
	CL	$\sim 8$			Netzer et al. (2002)
	XE, CL, BX	16 3–10		$\sim -1100$ $\sim -1100$	Turner et al. (2005)
NGC 3783	CH	$20.0^{+11.6}_{-1.4}$		$[-400, -600], [-1000, -1300]$	Netzer et al. (2003)
		$10.0^{+4.1}_{-2.9}$		$[-400, -600], [-1000, -1300]$	
		$7.9^{+2.1}_{-1.9}$		$[-400, -600], [-1000, -1300]$	
NGC 4051	CH	$\sim 1$		$-2340 \pm 130$	Collinge et al. (2001)
		$\sim 0.1$		$-600 \pm 130$	
	XE	$\sim 200$	$\sim 3.8$	$\sim -6500$	Pounds et al. (2004)
		$\sim 6$	$2.7 \pm 0.1$	$0 \pm 200$	
XE	$\sim 2$	$1.4 \pm 0.1$	$0 \pm 200$	Ogle et al. (2004)	
	[0.03,1]	[0,2.8]	$400 \pm 100$		
Mkn 766	CH			$0 \pm 160$	Sako et al. (2003) <sup>a</sup>
NGC 4593	CH, RX XR, CL	$5.4^{+1.5}_{-0.8}$	$\sim 2.5$	$-135 \pm 40$	McKernan et al. (2003a) Steenbrugge et al. (2003)
		$1.6 \pm 0.4$	$2.6 \pm 0.1$	$-400 \pm 120$	
		$0.1 \pm 0.05$	$0.5 \pm 0.3$	$-400 \pm 120$	
MCG-6-30-15	CH	$\sim 32$	$\sim 2.5$	$\sim 0$	Lee et al. (2001) <sup>b</sup>
		$\sim 5$	$\sim 0.7$	$\sim 0$	
	XR	$\sim 2$	2–3	$-1900 \pm 140$	Sako et al. (2003) <sup>a</sup>
$\sim 2$	0.5–2	$-150 \pm 130$			
IC 4329a	XR	$\sim 1.3$	$-1.4 \pm 0.1$	$\sim 0$	Steenbrugge et al. (2005a) <sup>c</sup>
		$\sim 0.3$	$0.6 \pm 0.1$	$[-100, -300]$	
		$6.6 \pm 0.4$	$\sim 1.9$	$[-200, 0]$	
		$2.0 \pm 0.5$	$2.7 \pm 0.1$	$[-140, +180]$	
NGC 5548	CL, CH	$2.5 \pm 0.5$	$2.3 \pm 0.1$	$-530$	Steenbrugge et al. (2005b) <sup>d</sup>
		$1.0 \pm 0.4$	$1.9 \pm 0.1$	$-530$	
		$0.6^{+0.9}_{-0.4}$	$-0.2 \pm 0.2$	$-530$	
Mkn 509	CH	$2.1^{+0.4}_{-0.5}$	$1.8^{+0.1}_{-0.2}$	$-200 \pm 100$	Yaqoob et al. (2003)
Akn 564	CH	$\sim 1$	$\sim 2$	$\sim -200$	Matsumoto, Leighley & Marshall (2004)
		$\sim 1$	$\sim 1$	$\sim -200$	

<sup>a</sup>Includes a model continuum component representing relativistically broadened O VIII Ly $\alpha$  or a radiative recombination continuum from material close to a Kerr BH. <sup>b</sup>Continuum model included a column density of  $3 \times 10^{17} \text{ cm}^{-2}$  of FeO<sub>2</sub>. <sup>c</sup>Continuum model included a blackbody with temperature of  $kT = 473 \text{ eV}$  and a neutral absorber with a column density of  $\sim 3 \times 10^{21} \text{ cm}^{-2}$ . <sup>d</sup>Used  $z = 0.01676$  from optical measurements rather than  $z = 0.01717$  from 21-cm H I measurements.

NGC 5448 were marginally blueshifted ([O VII] lay at an offset velocity of  $-265^{+160}_{-215} \text{ km s}^{-1}$ ), but the O VIII Ly $\alpha$  emission was marginally redshifted. The weighted mean offset velocity of the emitting material ( $-115 \pm 125 \text{ km s}^{-1}$ ) was consistent with emission at systemic velocity. NGC 3783 exhibited very strong O VIII Ly $\alpha$ , [Ne IX] and O VII (r) emission, the latter indicating that collisional ionization may be important in the emitting material Porquet et al. (2001), although photoexcitation due to high levels of UV flux could also account for O VII (r) emission Kinkhabwala et al. (2002). Also present were emission features due to [O VII] and O VII (i). The He-like forbidden emission lines in NGC 3783 were marginally

blueshifted, but the other emission lines were marginally redshifted. The weighted mean offset velocity of the emitting material was consistent with emission at systemic velocity.

The spectra of Mkn 279, NGC4593, Mkn 509 and Mkn 766 each exhibited several emission features, most prominently O VIII Ly $\alpha$  and/or [O VII], but they did not exhibit  $>2$  emission features at  $>99$  per cent significance. Out of the 10 AGN, we therefore only fit the spectra of NGC 3783, 4051 and 5548 with XSTAR models of emission. The best-fitting results are given in Table 5. The requirement that  $\Delta R/R < 1$  yields lower limits of  $n_e > 3.7 \times 10^6, 2.3 \times 10^2, 2.8 \times 10^2 \text{ cm}^{-3}$  for NGC 4051, 5548 and 3783, respectively.

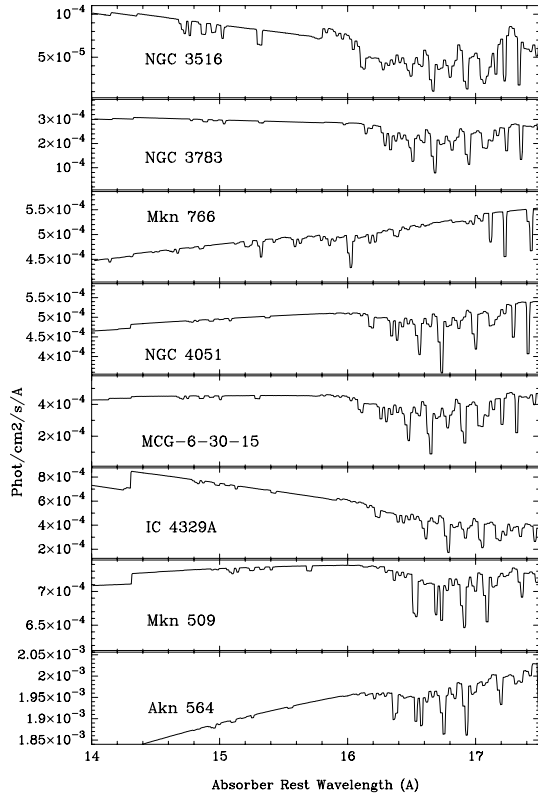


**Figure 5.** Plots of the model Fe UTAs produced by warm absorber components from Table 3 with best-fitting ionization parameters in the range  $\log \xi \sim 0.0 - 1.0$  (see the text).

**Table 5.** Properties of emitters.

Source	$N_{\text{em}}$ ( $10^{21} \text{ cm}^{-2}$ )	$\log \xi_{\text{em}}$ ( $\text{erg cm s}^{-1}$ )	$n_e^f$ ( $\text{cm}^{-3}$ )	$v_{\text{em}}$ ( $\text{km s}^{-1}$ )
NGC 3783	$2.4^{+1.1}_{-1.3}$	$1.61^{+0.15}_{-0.16}$	$>280$	$-5 \pm 45$
NGC 4051	$108^{+34}_{-88}$	$2.14^{+0.28}_{-0.40}$	$>3.7 \times 10^6$	$-160 \pm 75$
NGC 5548	$15.7^{+9.1}_{-13.6}$	$1.40^{+0.15}_{-0.36}$	$>230$	$-115 \pm 125$

<sup>a</sup>We used  $n_e = 10^8 \text{ cm}^{-3}$  as a default electron density since the data could not discriminate between emission model grids in the range  $10^2 - 10^{11} \text{ cm}^{-3}$ .

## 5 PROPERTIES OF THE WARM ABSORBERS IN TYPE I AGNs

The results of the photoionization modelling of the AGN spectra are summarized in Table 3. Figs 2–4 show the best-fitting photoionization models (from Table 3) superimposed on the AGN spectra. Our uniform analysis of the AGN sample has yielded warm absorber parameters ( $N_{\text{H}}$ ,  $\log \xi$ , velocity) that agree reasonably well with those in the literature (often from much more detailed analyses).

Our results provide the first overview of high-resolution soft X-ray grating data from *Chandra* observations of type I AGN. In summary, we found that nine out of the 15 AGN in the sample have intrinsic continua that are more complex than a simple power law in the 0.5–5.0 keV band (modelled here as a broken power law). Of the remaining six AGN spectra, the continua of three (F9, 3C 120 and Mkn 279) are well described by simple power-law models and the continua of the three remaining AGN (NGC 3227, 3516

and 7314) are well described by heavily absorbed power-law models. Note that previous, higher S/N data of the heavily absorbed AGN (NGC 3227 and 7314), evidence for photoionized absorption has in some cases been detected (see e.g. Ptak et al. 1994; George et al. 1998). The nine AGN spectra with complex intrinsic continua exhibit signatures of an ionized absorber as does the spectrum of NGC 3516, in spite of being heavily absorbed. The absorbers appear to be photoionized and outflowing, with velocities in the range  $\sim 0 - 2000 \text{ km s}^{-1}$  (similar to the speed of the solar wind). The column density of the warm absorbing gas is  $\sim 10^{20-23} \text{ cm}^{-2}$ . Nine out of the 10 AGN exhibiting warm absorption are best fitted by multiple ionization components and three out of the 10 AGN require multiple kinematic components. The warm absorbing gas in our AGN sample has a wide range of ionization states, spanning roughly four orders of magnitude ( $\xi \sim 10^0 - 10^4$ ) and up to three orders of magnitude in the same source. Out of the 10 AGN spectra that exhibit warm absorption, a simple fit to the 0.5–0.7 and 2.5–5.0 keV energy regions reveals that the intrinsic continuum of two AGN (NGC 4051 and 5548) exhibits a statistically significant upturn in the intrinsic soft X-ray continuum relative to a hard X-ray power law. Our simple test shows that MCG-6-30-15 does not require a soft excess. The remaining AGN that exhibit warm absorption are either heavily absorbed in soft X-rays or exhibit spectral complexity that cannot be accounted for by such a naive test of the data. Nine out of the 10 AGN that exhibit warm absorption also exhibit Fe UTAs, indicative of an absorber component that could (depending on absorber density and geometry) carry most of the mass in outflow, as we show below.

Fig. 6 compares the warm absorber component parameters from the different AGN (see Tables 3 and 5). Fig. 6(a) shows the relationship between warm absorber outflow velocity and the corresponding warm absorber column density. Clearly the warm absorber components in all 10 AGN are outflowing and with velocities that span around two orders of magnitudes. There appears to be a gap in the outflow velocities in our sample between  $\sim 300$  and  $500 \text{ km s}^{-1}$ , the origin of which is not clear. The outflow components with velocities below this gap tend to be associated with lower column densities than those with velocities above the gap. Fig. 6(b) shows that the ionization parameter of the warm absorber is independent of velocity and can vary by up to three orders of magnitude in the same source, suggesting that the outflowing absorber components consist of gas lying at different points on the heating/cooling curve (e.g. Krolik & Kriss 2001). Furthermore Fig. 6(b) also indicates that there is a separate population of low ionization state absorber components at  $\xi < 10$ . These low ionization parameter absorber components are responsible for the Fe UTAs in the AGN spectra. One caveat is that there is no bias in principle in the X-ray band for absorbers with ionization states  $10 < \xi < 100$ ; however, *Chandra* HETGS is less sensitive than other instruments to this band.

The warm absorber outflow apparent in 10 out of the 15 AGN in our sample must clearly carry mass away from the central SBH. The rate of mass-loss from an AGN outflow is given by

$$\dot{M}_{\text{outflow}} = \left( \frac{\Delta\Omega}{4\pi} \right) C y m_p n_e v 4\pi r^2, \quad (1)$$

where  $\Delta\Omega$  is the solid angle subtended by the absorber at the ionizing source,  $C$  is the volume filling factor,  $y$  is the mean atomic mass per hydrogen atom ( $y \sim 1.3$  for solar abundances),  $m_p$  is the proton mass,  $n_e$  is the electron density of the absorber,  $r$  is the distance of the absorber from the radiation source and  $v$  is the outflow velocity. We believe that the filling factor,  $C$ , cannot be reliably constrained by current observations of AGN (see e.g. discussion in Section 5.1).

**Table 6.** Black hole masses for AGN with warm absorbers. Column 2 lists the 0.5–2.0 keV luminosity for each source, corrected for absorption.

Source	0.5–2.0 keV luminosity ( $10^{43}$ erg s $^{-1}$ )	$L_{\text{ion}}$ ( $10^{44}$ erg s $^{-1}$ )	$M_{\text{BH}}$ ( $10^6 M_{\odot}$ )	$L_{\text{ion}}/L_{\text{edd}}$	Reference
NGC 3516 (low)	0.16	0.15	43	0.003	1
NGC 3516 (high)	0.38	0.36	–	0.007	1
NGC 3783	1.25	1.00	30	0.003	1
NGC 4051	0.02	0.02	2.0	0.006	1
Mkn 766	0.66	0.47	0.6	0.572	2
NGC 4593	0.50	0.29	5.4	0.042	1
MCG-6-30-15	0.32	0.16	4.5	0.027	3
IC 4329A	0.76	3.40	7.5	0.349	1
NGC 5548	6.98	0.83	96	0.007	1
Mkn 509	6.55	5.23	100	0.040	1
Akn 564	6.54	4.69	1.2	3.000	4

References: (1) Peterson et al. (2004); (2) Botte et al. (2005); (3) McHardy et al. (2005); (4) Bian & Zhao (2003).

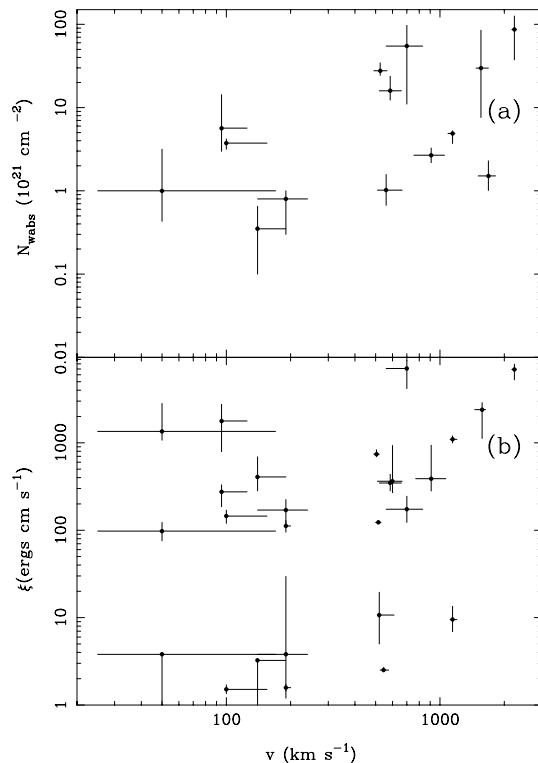


**Figure 6.** Velocity of warm absorber components (a) versus column density ( $N_{\text{H}}$ ) and (b) versus  $\xi$  of warm absorber component for the AGN in our sample (from Table 3). In panel (a), we plot the total column density of all the warm absorber components around a particular velocity. Thus, for example, the three low-velocity components from NGC 3783 in Table 3 become a single velocity component between  $-490$  and  $-565$  km s $^{-1}$  in panel (a). In panel (b), we plot *all* the individual warm absorber components to illustrate the fact that the ionization parameter can vary by up to three orders of magnitude in the same source. In panel (b), the low ionization components ( $\xi < 10$ ) correspond to the Fe UTAs.

Blustin et al. (2005) estimated  $C$  for a sample of sources based on various assumptions, but those same assumptions led Blustin et al. (2005) to derive a maximum distance between the absorber and radiation source that was *less* than the minimum distance for no less than five sources. On the other hand, it is possible to argue

that the covering factor ( $\Delta\Omega/4\pi$ ) is approximately equal to the fraction of type I AGN in which a warm absorber is detected, or  $\sim 0.5 - 0.7$ . However, this argument breaks down if AGN winds are accelerating and/or ‘bend’, rather than constant velocity, non-accelerating outflows. Even so, this still leaves  $C$  (and therefore the mass outflow rate) unconstrained. From the definition of the ionization parameter,  $r^2 = L_{\text{ion}}/n_e \xi$ , therefore

$$\dot{M}_{\text{outflow}} = 16.6xy \left( \frac{\Delta\Omega}{4\pi} \right) \frac{L_{\text{ion},44}}{\xi_{100}} v_{500} C M_{\odot} \text{ yr}^{-1}, \quad (2)$$

where  $L_{\text{ion},44} = L_{\text{ion}}/10^{44}$ ,  $\xi_{100} = \xi/100$  and  $v_{500} = v/500$  where  $v$  is the outflow velocity,  $y$  is the mean atomic mass per hydrogen atom and  $x$  is the number of hydrogen atoms per free electron. With  $x = 9/11$  and  $y = 1.3$ , the product  $xy$  is approximately unity, or  $\sim 1.06$ . Equation (2) suggests that all else being equal, warm absorbing gas with a low value of ionization parameter should account for the largest mass outflows from AGN. Table 6 lists the value of  $L_{\text{ion}}$ , SBH mass and 0.5–2.0 keV luminosity for each AGN in Table 3. From Table 3 we find mass outflow rates in the range  $\sim 10^{-1}$  to  $10^3 \times (\Delta\Omega/4\pi) C M_{\odot} \text{ yr}^{-1}$ . Therefore, even for small filling factors, the outflow rate can be comparable to the expected accretion rate on to the central SBH. The accretion rate on to the black hole is  $\dot{M}_{\text{accretion}} = L_{\text{bol}}/\eta c^2$ , where  $L_{\text{bol}}$  is the bolometric luminosity of the AGN and  $\eta$  is the accretion efficiency of the black hole. If  $L_{\text{bol}} = 10 X_{10} L_{\text{ion},44}$ , where  $X_{10}$  is a parameter of the order of unity, and  $\eta = 0.1\eta_{0.1}$ , then  $\dot{M}_{\text{accretion}} = L_{\text{ion},44} X_{10} / (5.7 \times \eta_{0.1}) M_{\odot} \text{ yr}^{-1}$  and

$$\frac{\dot{M}_{\text{outflow}}}{\dot{M}_{\text{accretion}}} \sim 94 \left( \frac{\Delta\Omega}{4\pi} \right) \left( \frac{xy}{X_{10}} \right) \left( \frac{v_{500}}{\xi_{100}} \right) \eta_{0.1} C. \quad (3)$$

The value of  $C$  and the covering factor of the absorber is critical to understanding the processes underpinning the warm absorption phenomenon. If  $v_{500}, X_{10}, \eta_{0.1} \sim 1$  and if  $(\Delta\Omega/4\pi) \sim 0.5$  typically, then the filling factor must be very small ( $< 0.02$ ) for the mass outflow rate to be comparable to or less than the accretion rate (a point also made by Steenbrugge et al. 2005b).

The warm absorber components found in Seyfert 1 galaxies have column densities that are too small to account for the EWs of the narrow, core, Fe K line emission. However, for our sample, we investigated whether the core Fe K line emission EW correlate with the column densities of the warm absorber components in case of a secondary effect. For example, if the warm absorber material is an outflow of material from the putative obscuring torus, and if the core

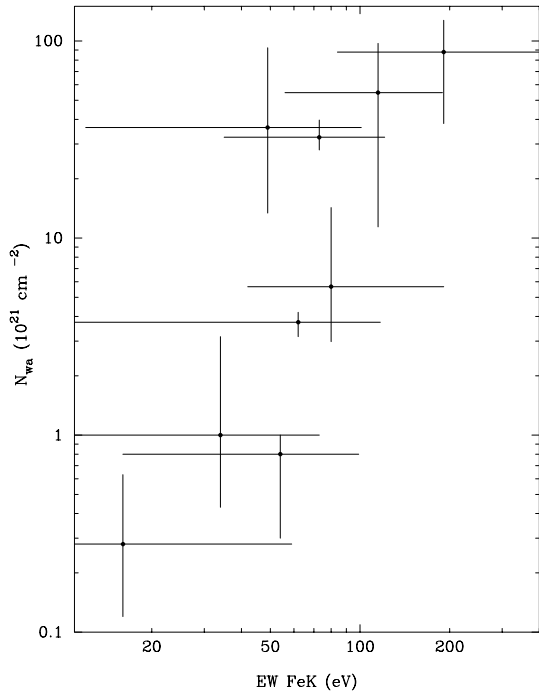


**Figure 7.** EW of the Fe  $K\alpha$  line in each AGN versus the total warm absorber column density (from Table 5). Fe  $K\alpha$  measurements were taken from Yaqoob & Padmanabhan (2004). A weak correlation between total column density of absorber and the EW of the Fe  $K\alpha$  line is permitted; however, Fe  $K\alpha$  line EWs can vary significantly in individual AGN, so a correlation is unlikely.

Fe K line emission originates in the torus itself, one might expect a correlation between the Fe K line EW and the warm absorber column density if thicker torii produce thicker winds. We also investigated whether the Fe  $K\alpha$  line in type I AGN ‘knows’ about the warm absorber by comparing the total column density of the warm absorber in an AGN with the EW of the corresponding core Fe  $K\alpha$  line (Yaqoob & Padmanabhan 2004) (Fig. 7).

For our sample, Fig. 7 shows the EW measurements (from Yaqoob & Padmanabhan 2004) versus warm absorber column density. A weak correlation is permitted based on Fig. 7, so the Fe  $K\alpha$  line might ‘know’ about a large warm absorber column density. In this case we calculate the Pearson correlation coefficient to be 0.88 (for  $N = 9$ ), which is significant at the  $\sim 99$  per cent confidence level. However, we caution that the EWs of individual Fe  $K\alpha$  lines can vary by a factor of 2–3 as the continuum varies whilst the line intensity does not, and this would destroy any hint of correlation in Fig. 7, which may therefore be spurious. In particular, we note that no warm absorber is detected in F9, yet it *has* a prominent, strong Fe  $K\alpha$  line core (Yaqoob & Padmanabhan 2004).

### 5.1 Comparison with other AGN sample studies

Blustin et al. (2005) collated from the literature the results of some of the X-ray spectral observations of 23 AGN using *Chandra* and *XMM-Newton* and attempt to infer the general properties of Seyfert warm absorbers from these results. The methodology of the Blustin et al. (2005) study is quite different from the present work. However, the strengths of our study (uniform analysis and a single instrument) may also be weaknesses. Our selection criteria for warm absorption signatures may be too conservative, our uniform modelling of the

continuum may ignore individual source peculiarities and our band-pass may miss, for example, very low ionization absorber components. A study such as the one carried out by Blustin et al. (2005) is a useful comparison for these reasons. Blustin et al. (2005) conclude that most warm absorbers are most likely to originate in outflows from the dusty torus, since they estimate that the minimum distance of the warm absorbers from the central radiation source mostly cluster around the distance of the torus. Blustin et al. (2005) conclude that the kinetic luminosity of these outflows is  $< 1$  per cent of the AGN bolometric luminosity and the observed soft X-ray absorbing ionization phases fill  $< 10$  per cent of the available volume.

Some of the conclusions reached by Blustin et al. (2005) are quite different from ours. We make no claim for the filling factors of the outflows or indeed, their origin. First, we believe there are currently insufficient data and constraints to reliably estimate the filling factor, preventing the derivation of absolute mass outflow rates. Secondly, we note that Blustin et al. (2005) calculate a minimum distance between the central radiation source and the warm absorber based only on the assumption that the outflow velocity exceeds the escape velocity. However, very recently Miller et al. (2006) observed an X-ray absorbing outflow from the stellar mass black hole binary GRO J1655–40 with a radial velocity *far less* than the escape velocity at its location. Moreover, the assumptions of Blustin et al. (2005) lead to a maximum distance of the warm absorber from the radiation source that is *less* than the minimum distance for no less than five AGN. Robust information on the distance between the warm absorber and the central source can only come from variability studies of the absorber. Thirdly, Blustin et al. (2005) conclude that Seyfert warm absorbers are probably not telling us anything fundamental about the energetics or structure of the central engine. However, if for example, warm absorbers originate in a disc wind, the properties of the disc wind are likely to correlate with those of the disc (magnetic flux strength, disc temperature gradient, velocity of disc, etc.). Finally, some parts of the warm absorbing outflows from AGN discussed here and by Blustin et al. (2005) *may not actually be observable* because they are fully ionized. Such fully ionized outflows may be the fastest component of the outflow since it may be closest to the source of ionizing radiation.

## 6 DISCUSSION

At present there are two distinct theories of the origin of the warm absorber. On one hand, Elvis (2000) proposes a unified scheme for quasars that includes a wind that rises vertically from a narrow range of radii on the inner accretion disc and is then bent outwards by a radial radiation force to produce a funnel-shaped thin shell outflow. This model specifically excludes the dusty molecular torus as a characteristic of AGN and proposes that the Fe  $K\alpha$  emission line is produced in the funnel. Elvis (2000) predicts that the range of linewidths will be similar to the broad absorption-line ‘detachment velocities’ ( $\sim 0 - 5000$  km  $s^{-1}$  vertically, so one might expect a narrower linewidth than this when looking down the funnel). Out of the 48 absorption features used to constrain the warm absorber components in this study, 37 have FWHM  $< 2000$  km  $s^{-1}$  and only four allow for FWHM  $> 3000$  km  $s^{-1}$ . Statistically, a weak correlation is allowed between the EW of the Fe  $K\alpha$  line and the total column density of the warm absorber. However, we note that in our sample, the source with the least evidence for *any* warm absorption (F9) exhibits the largest Fe  $K\alpha$  EW, which is not consistent with expectations from the Elvis model.

On the other hand, Krolik & Kriss (2001) propose that the warm absorber originates in a photoionized evaporation from the inner

edge of the putative obscuring torus believed to surround the AGN central engine. In this model, the warm absorber is a multitemperature wind, with the different outflow components having values of  $\Xi$  (pressure form of ionization parameter) that cover a relatively narrow range, as a result of the different phases of gas co-existing in pressure equilibrium. From our photoionization model fits, we find that the temperatures of the warm absorber components lie in the range  $T \sim 10^4 - 10^7$  K for the sample, yet  $\log \Xi$  lies in the range  $\sim 0 - 1$ , with the highest ionization components generally having the largest values of  $T$  and  $\Xi$ . Thus, our general constraints seem to agree quite well with the model predictions of Krolik & Kriss (2001). An additional attraction of this model is that the interaction of the disc wind with the dusty molecular torus in this model can also naturally explain dusty warm absorption, which may be the cause of additional spectral complexity of some of the AGN in this sample (see Section 3).

One important point to note is that some of the warm absorber components discussed above may actually be due in part to hot local gas at  $cz \sim 0$ . For example, the low-velocity warm absorber component in NGC 4051 at ( $\sim -600$  km s $^{-1}$ ) is kinematically very close to an absorption signature at  $cz \sim 0$  since NGC 4051 is cosmologically redshifted by  $cz = 726 \pm 15$  km s $^{-1}$  from  $z \sim 0$ . Other AGN in this sample yield tantalizing hints of absorption due to hot local gas (see McKernan, Yaqoob & Reynolds 2004, 2005 and references therein for further details). Of course, the absorption signatures of some of the warm absorbing outflows could be mimicked by hot gas at intermediate redshift. However, the expected column density of most filaments of warm/hot intergalactic medium (Cen & Ostriker 1999) is far lower than that observed by us.

The soft X-ray spectra of type I AGN observed with the high-resolution *Chandra* and *XMM-Newton* observatories prompt many intriguing questions. We believe that these questions can be answered only by careful uniform analysis of a sample of AGN. Our uniform analysis has its limitations since we use spectra from only one instrument with a limited bandpass, and our methodology is sufficiently conservative that we may miss less significant absorber signatures. Nevertheless, we have carried out a first uniform analysis on a small sample of AGN observed with *Chandra* HETGS and we have established reasonably well-constrained parameter ranges for the warm absorbing outflows in type I AGN. Interestingly, we found that mass-loss resulting from the warm absorber outflow can be high, comparable to or greater than the expected accretion rate on to the central SBH. Most of the outflowing mass could be carried by low ionization state outflows (depending on absorber density and geometry), which are best studied in the X-ray band via their Fe UTA spectral imprint. Low rates of mass outflow from AGN and higher velocity outflows may be associated with lower values of the AGN Eddington ratio, but the rate of mass outflow does not correlate with the mass of the central black hole. A weak contribution to the core of the narrow Fe K $\alpha$  line from high column density warm absorbers seems unlikely. There is a gap in the outflow velocities of the warm absorber components in the range  $\sim 300 - 500$  km s $^{-1}$ , which is puzzling. All these results so far provide tantalizing hints at global patterns of type I AGN behaviour and merit further investigation using a larger sample of high spectral resolution AGN spectra.

## ACKNOWLEDGMENTS

BM gratefully acknowledges support from NSF grant AST0205990. TY acknowledges support from NASA through grant AR4-5009X issued by *Chandra* X-ray Observatory Center, operated by the SAO

for and on behalf of NASA under contract NAS8-39073. We made use of the HEASARC online data archive services, supported by NASA/GSFC and also of the NED, operated by the Jet Propulsion Laboratory, CalTech, under contract with NASA. Thanks to the *Chandra* instrument and operations teams for making the observations possible. Thanks to Tim Kallman for numerous useful discussions on XSTAR. Thanks to the anonymous referee for very detailed and useful comments that helped to improve and shorten this paper. Thanks to Fabrizio Nicastro for discussing his results from an unpublished *XMM-Newton* RGS observation of NGC 4051.

## REFERENCES

- Arav N., Korista K. T., de Kool M., 2002, *ApJ*, 566, 699  
 Behar E., Netzer H., 2002, *ApJ*, 570, 165  
 Behar E., Sako M., Kahn S. M., 2001, *ApJ*, 563, 497  
 Bian W., Zhao Y., 2003, *MNRAS*, 343, 164  
 Blustein A. J., Branduardi-Raymont G., Behar E., Kaastra J. S., Kahn S. M., Page M. J., Sako M., Steenbrugge K. C., 2002, *A&AS*, 392, 453  
 Blustein A. J., Page M. J., Fuerst S. V., Branduardi-Raymont G., Ashton C. E., 2005, *A&AS*, 431, 111  
 Botte V., Ciroi S., diMille F., Rafanelli P., Romano A., 2005, *MNRAS*, 356, 789  
 Branduardi-Raymont G., Sako M., Kahn S. M., Brinkman A. C., Kaastra J. S., Page M. J., 2001, *A&AS*, 365, 140  
 Cash W., 1976, *A&AS*, 52, 307  
 Cen R., Ostriker J. P., 1999, *ApJ*, 514, 1  
 Collinge M. J. et al., 2001, *ApJ*, 557, 2  
 Crenshaw D. M., Kraemer S. B., 1999, *ApJ*, 521, 572  
 Elvis M., 2000, *ApJ*, 545, 63  
 Elvis M., Wilkes B. J., Lockman F. J., 1989, *AJ*, 97, 777  
 Ferland G. J., Martin P. G., van Hoof P. A., Weingartner J. C., 2002, Workshop on X-ray Spectroscopy of AGN with *Chandra* and *XMM-Newton*, held at MPE Garching, December 3–6, 2001, Report 279, p. 103  
 Gehrels N., 1986, *ApJ*, 303, 336  
 George I. M., Turner T. J., Netzer H., Nandra K., Mushotzky R. F., Yaqoob T., 1998, *ApJS*, 114, 73  
 Halpern J. P., 1984, *ApJ*, 281, 90  
 Kaastra J. S., Steenbrugge K. C., Raassen A. J. J., van der Meer R. L. J., Brinkman A. C., Liedahl D. A., Behar E., de Rosa A., 2002, *A&AS*, 386, 427  
 Kinkhabwala A. et al., 2002, *ApJ*, 575, 732  
 Krolik J. H., Kriss G. A., 2001, *ApJ*, 561, 684  
 Lee J. C., Ogle P. M., Canizares C. R., Marshall H. L., Schulz N. S., Morales R., Fabian A. C., Iwasawa K., 2001, *ApJ*, 554, L13  
 McHardy I. M., Gunn K. F., Uttley P., Goad M. R., 2005, *MNRAS*, 359, 1469  
 McKernan B., Yaqoob T., George I. M., Turner T. J., 2003a, *ApJ*, 593, 142  
 McKernan B., Yaqoob T., Mushotzky R., George I. M., Turner T. J., 2003b, *ApJ*, 598, L83  
 McKernan B., Yaqoob T., Reynolds C. S., 2004, *ApJ*, 617, 232  
 McKernan B., Yaqoob T., Reynolds C. S., 2005, *MNRAS*, 361, 1337  
 Markert T. H., Canizares C. R., Dewey D., McGuirk M., Pak C., Shattenburg M. L., 1995, *Proc. SPIE*, 2280, 168  
 Mason K. O. et al., 2003, *ApJ*, 582, 95  
 Matsumoto C., Leighley K. M., Marshall H. L., 2004, *ApJ*, 603, 456  
 Matt G., 1994, *MNRAS*, 267, L17  
 Miller J. M., Raymond J., Fabian A., Steeghs D., Homan J., Reynolds C., van der Klis M., Wijnands R., 2006, *Nat*, 441, 953  
 Morales R. M., Fabian A. C., 2002, *MNRAS*, 329, 209  
 Murphy E. M., Lockman F. J., Laor A., Elvis M., 1996, *ApJS*, 105, 369  
 Nandra K., Pounds K. A., 1992, *Nat*, 359, 215  
 Netzer H., Chelouche D., George I. M., Turner T. J., Crenshaw D. M., Kraemer S. B., Nandra K., 2002, *ApJ*, 571, 256  
 Netzer H. et al., 2003, *ApJ*, 599, 933

- Ogle P. M., Mason K. O., Page M. J., Salvi N. J., Cordova F. A., M<sup>c</sup>Hardy I. M., Priedhorsky W. C., 2004, *ApJ*, 606, 151
- Peterson B. M. et al., 2004, *ApJ*, 613, 682
- Porquet D., Mewe R., Dubau J., Raassen A. J. J., Kaastra J. S., 2001, *A&AS*, 376, 1113
- Pounds K. A., Reeves J. N., Page K. L., Edelson R., Matt G., Perola G. C., 2003, *MNRAS*, 341, 953
- Pounds K. A., King A. R., Reeves J. N., Page K. L., 2004, *MNRAS*, 350, 10
- Ptak A. F., Yaqoob T., Serlemitsos P. J., Mushotzky R., Otani C., 1994, *ApJ*, 436, L31
- Reynolds C. S., 1997, *MNRAS*, 286, 513
- Reynolds C. S., Nowak M. A., 2003, *Phys. Rep.*, 377, 389
- Sako M. et al., 2001, *A&AS*, 365, L168
- Sako M. et al., 2003, *ApJ*, 596, 114
- Steenbrugge K. C. et al., 2003, *A&AS*, 408, 921
- Steenbrugge K. C., Kaastra J. S., Sako M., Branduardi-Raymont G., Behar E., Paerels F. B. S., Blustin A. J., Kahn S., 2005a, *A&A*, 432, 453
- Steenbrugge K. C. et al., 2005b, *A&A*, 434, 569
- Turner T. J., Nandra K., George I. M., Fabian A. C., Pounds K. A., 1993, *ApJ*, 419, 127
- Turner T. J., Kraemer S. B., Mushotzky R. F., George I. M., Gabel J. R., 2003, *ApJ*, 594, 128
- Turner T. J., Kraemer S. B., George I. M., Reeves J. N., Bottorff M. C., 2005, *ApJ*, 618, 155
- Ward M., Elvis M., Fabbiano N., Carleton P., Willner S. P., Lawrence A., 1987, *ApJ*, 315, 74
- Yaqoob T., Padmanabhan U., 2004, *ApJ*, 604, 63
- Yaqoob T., McKernan B., Kraemer S. B., Crenshaw D. M., Gabel J. R., George I. M., Turner T. J., 2003, *ApJ*, 582, 105

This paper has been typeset from a  $\text{\TeX}/\text{\LaTeX}$  file prepared by the author.